Channel Distortion to QR Codes

Matias A. Botoluzzi, Alexandre Campos, Osmar M. dos Santos, Andrei P. Legg and Renato Machado

***Abstract*— In this paper we analyze the distortion limits of the Quick Response (QR) code decoder (available in Google open-source 1D/2D barcode image processing library Zxing-2.1) under common sources of camera channel impairments which are: motion and defocus blur, lighting reduction, barrel and pincushion distortion, Gaussian and salt and pepper noise. Tests are conducted in a controlled scenario where black and white QR code was subject to real world distortions taken individually. Image degradation was evaluated in terms of synchronization success rate (SSR) and peak signal-to-noise ratio (PSNR). We concluded that QR code is more robust against pincushion distortion, where the SSR is obtained with only 5.58 dB of PSNR.**

***Keywords*— QR code, camera channel, image degradation, synchronization success rate.**

I. Introduction

In the past years, mobile phones have the data input restrict to phones' numerical keypads [1]. Nowadays, with the advent of smartphones data input come also from microphones and digital cameras. Usually, cameras are used to produce selfies and short movies, commonly shared with friends in virtual communities using social media platforms. However, smartphone cameras can also interact with time-invariant short codes (e.g. barcodes) being interpreted as a part of a communication system [2, 3]. Historically one of the first commercial barcode was the one-dimensional (1D) Universal Product Code (UPC) [4] which consists of interleaved vertical black lines separated by white spaces. However the necessity of increasing information density in a limited space led to the development of a black and white two-dimensional (2D) barcode [5]. 2D barcode is an automatic identifiable graphical image that stores information in both dimensions, horizontal and vertical [6] pursuing higher density, capacity and reliability. QR code standard [7] is a 2D barcode most used around world thanks to its robustness and several commercial applications [8].

However, even images acquired from QR codes are subject to many distortions such as noise, blur, rotation, perspective, uneven illumination, or partial code area occlusion [9], among other problems. Therefore, new barcode symbologies and existing 2D barcodes should be robust to distortions to facilitate the decoding process.In this study we use the QR code decoder in order to evaluate its performance considering some image acquisition distortions.

The rest of this paper is organized as follows: Section II presents the standard QR code structure. Then, in Section III, we summarize the common image channel impairments that degrade the barcode, and their mathematical model. Finally, Section IV and V build up a discussion and summarizes the contributions of this paper.

Matias A. Bortoluzzi, Andrei P. Legg, Osmar M. dos Santos, Alexandre Campos, Department of Electronics and Computing (DELC), Federal University of Santa Maria (UFSM), Santa Maria-RS, Brazil, and Renato Machado, Department of Telecommunications, Aeronautics Institute of Technology (ITA), São José dos Campos-SP, Brazil. E-mails: matiasbortoluzzi@gmail.com, alexandre@gedre.ufsm.br, osmar@inf.ufsm.br, andrei.legg@gmail.com, rmachado@ita.br.

II. QR code

QR code together with DataMatrix [10] were the pioneers in mobile applications. QR code is one kind of two dimensional matrix code developed by the Japanese Denso company in 1994 [11]. QR code is recognized by AIM Standard, JIS Standard and ISO Standard and is composed by forty versions, whose modules number (N_{mod}) depends on the version (V): $N_{mod} = 21 + 4 \times (V - 1)$. Furthermore, the maximum data capacity is limited to either 7089 numeric data, or 4296 alphanumeric data (more about data capacity is given in [7]). QR code symbol is composed by two structures: encoding region and function patterns (see Fig. 1).

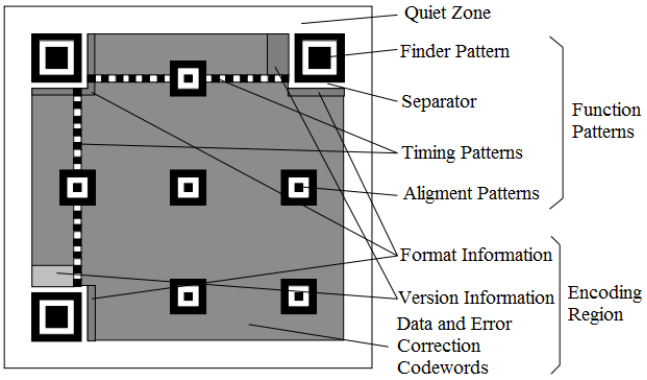

Fig. 1. Structures and substructures of the QR code version 7 [7].

The encoding region is composed by data and redundancy codewords (sequence of eight bits), version and format information which are described as follows:

- Data: QR code standard allows the following data modes: numeric, alphanumeric, byte (ISO/IEC 8859-1 character set) and Kanji.
- Redundancy: QR code uses Reed-Solomon (RS) channel coding algorithm to insert controlled redundancy. Four error correction (EC) levels are defined in the QR code: L, M, Q and H with symbols correction capacity of approximately 7%, 15%, 25% and 30%, respectively. QR code data storage varies in accordance with the version and also with the EC level [12].
- Format Information: sequence of fifteen bits comprised of five data bits and ten redundancy bits, using *Bose-Chaudhuri-Hocquenghem* code - BCH (15,5). The first five bits carry the EC level and mask information.

- Version Information: sequence of six bits representing one out of forty QR code versions, and twelve bits of redundancy BCH (18,6) code. Both version and format information have spatial redundancy as seen in Fig. 1.

Functions pattern are QR code invariant structures. These functions are briefly described as follows:

- Finder pattern: three identical finder patterns area located at the symbol corners, and composed by concentric squares with dimensions 7×7, 5×5 and 3×3. Their widths follow the ratio $1:1:3:1:1$ in unit of modules.
- Separator: one-module wide separator placed between each finder pattern and the Encoding Region.
- Quiet zone: a light surrounding region that facilitates the extraction of barcode from background.
- Timing pattern: alternating light and dark modules which brings information of the symbol density and QR code version.
- Alignment pattern: three superimposed concentric squares of 5×5 dark modules, 3×3 light modules and a single central dark module present only in Version 2 or larger. Those modules are used by the receiver to correct distortions.

Fig. 2 summarizes the standard QR code encoding process. The encoder recognizes the input data and classify it into the most efficient data mode. The coding converts the string of characters into a serial binary string. Then the RS encoder generates parity symbols in accordance with the EC levels. Information and parity symbols are placed in the QR code matrix by using codewords, starting from bottom right-hand corner to left. In order to avoid the finder pattern sequence "$1:1:3:1:1$" and to have more evenly balanced dark and light modules eight masks are applied to the barcode. Based on four penalties, one out of eight masks is chosen, the one that provides the best decoding performance. Finally, the format and version information are inserted in the QR code.

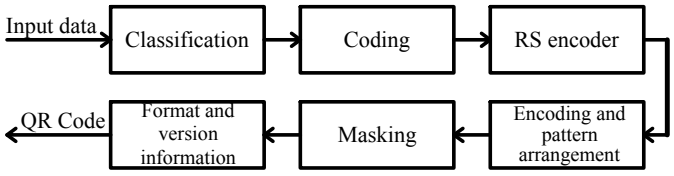

Fig. 2. Block diagram of a standard QR Code encoder (adapted from [12]).

Conversely Fig. 3 shows the decoding process starting from an image captured by a digital camera. The first step called module recognition aims to convert each recognized color patch into a binary matrix. Based on their luminance, the QR code patches are classified either in dark ("1") or light ("0"), using the following global threshold [12]:

$$L = \frac{L_{max} + L_{min}}{2}, \tag{1}$$

where L_{max} and L_{min} are the maximum and minimum luminance in a captured image, respectively.

Based on (1) the decoder starts searching for three finder patterns to detect the QR code. Once the finder and alignment

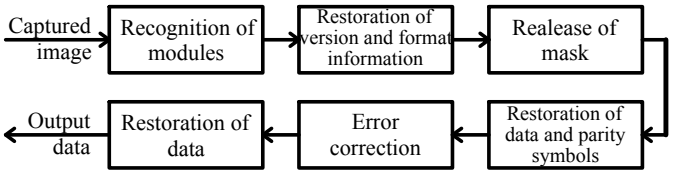

Fig. 3. Block diagram of a standard QR Code decoder (adapted from [12]).

patterns were detected, the decoder minimizes the geometric distortions mainly caused by mismatching alignment between camera lens and the QR code plan. Then, format and version information are obtained from the QR code and used in the decoding process. Recognized modules are unmasked and damage modules are restored through RS decoder. Finally, the remaining bit string is converted back into a data mode and the original data is recovered.

III. Channel Distortion Model

Usually, the barcodes captured by smartphones suffer distortions caused by the shooting process [13]. Lin and Fuh [14] highlight two important challenges in the decoding process: image acquired under nonuniform background, or uneven light, and/or shotting angle which might cause perspective distortion. Furthermore, distortions like mark, missing part, barcode on cylindrical surface area [6], noise and blurring at the time of image acquisition [15] make hard the task of recovering data from the corrupted images of the barcode. In general, blur can be caused by several factors such as incorrect focus (inaccurate focal length adjustment), motion (camera shaking while capturing an image), image captured in long-distance, inaccurate barcode boundary identification, and perspective projection or a combination of these factors [16].

A camera shooting process may be interpreted as part of a communication system as shown in Fig. 4. Transmitter is either a source light or a printed surface (reflected light) and the receiver is a smartphone. An overall channel model can be described by [17]:

$$g(i,j) = J\{C[D(h * W(f(x,y)))] + \eta(i,j)\}, \tag{2}$$

where:

- $g(i,j)$ is the degraded output image as result of the channel impairments over the clean input image $f(x,y)$;
- W is a warping function representing the geometrical transformation applied to the barcode image corresponding to camera orientation. W transform $f(x,y)$ into $f^w(i,j)$;
- h denotes the point spread function (PSF) of the channel, and $*$ convolution;
- D is the CMOS sensor function that distort the image, in two ways: 1) a sensor PSF and a sampling function and 2) a nonlinear response to light plus color crosstalk;
- C depicts the digital signal processing applied by the camera software, because of the off-the-shelf cell phone cameras are designed to capture personal

images, based on eye sensibility which is not linear and is more sensitive to luminance;

η is the additive white Gaussian noise (AWGN); and finally

J describes the inner JPEG compression.

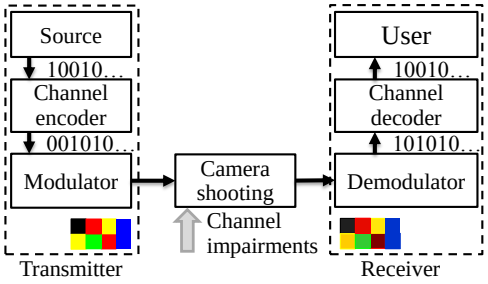

Fig. 4. Description of a camera shooting process as a communication system (adapted from [18]).

In this paper we evaluate only the effects of noise (η) and PSF degradation (h). Therefore we rewrite (2) as follows [19]:

$$g(x,y) = h(x,y) * f(x,y) + \eta(x,y), \tag{3}$$

where $g(x,y)$ is the degraded image in spatial domain.

In the frequency domain (3) is given by

$$G(x,y) = H(x,y) \cdot F(x,y) + N(x,y). \tag{4}$$

Function $h(x,y)$ is defined by the hardware of the imaging system, and it does not change once the system was designed. It reveals the point spread function (PSF), or impulse response of the system. Both blurring (motion and defocus blur) and radial lens distortion (barrel and pincushion) are modeled by PSF. On the other hand, noise is a sub-product of digitalization and/or transmission process and it has a stochastic nature.

A. Blurring Models

An image in which the focal point falls exactly on the focal plan in a single dot is in sharp focus. However, when the focal point falls before or after of the focal plan the dot grows up into a disk called circle of confusion (COC). Therefore an object is out-of-focus when the COC diameter in the image plane is larger than one pixel. In general, camera defocus blur can be modeled as a uniform disk with radius R in the following way [20]:

$$h_{defocus}(x,y) = \begin{cases} \frac{1}{\pi R^2}, \text{if } \sqrt{x^2+y^2} \leq R, \\ 0, \text{ otherwise.} \end{cases} \tag{5}$$

Nonetheless, motion blur can be modeled by considering two parameters: angle (α) and length (L). In this study, we consider only translation, the most relevant type of motion blur, where either the object or camera is translated in a constant and relative velocity v, during an exposure interval T, with an angle α from the horizontal axis. Expressing $L = v \times T$ we can describe the motion blur effect as [21]:

$$h_{motion}(x,y) = \begin{cases} \frac{1}{L}, \text{if } \sqrt{x^2+y^2} \leq \frac{L}{2} \text{ and } \frac{x}{y} = -\tan\alpha, \\ 0, \text{ otherwise.} \end{cases} \tag{6}$$

Finally, if both defocus and motion blur are present, then the degradation function is given by

$$h(x,y) = h_{defocus}(x,y) * h_{motion}(x,y). \tag{7}$$

B. Lens Distortion Model

An important property of *pinhole* (camera without lens) model is that the 3D lines of the scene are projected over 2D lines in an image plane. Unfortunately the lens, specially those of low cost, can introduce interferences in straight transmissions. Such shortcomings are named as barrel and pincushion distortions which are illustrated in Fig. 5.

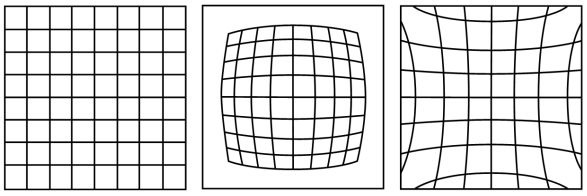

Fig. 5. From left to right: no distortion, barrel and pincushion distortions (extracted from [22]).

The distortion of the lenses is radial and the simplest way to model is through a shift of the distance for every pixel from the image center [22]. We denote r_u and r_d as distances of the undistorted and distorted images coordinates from de image center, respectively. Therefore, the radial distortion is often modeled by Taylor expansion [23]:

$$r_u = r_d(1 + k_1 r_d^2 + k_2 r_d^4 + \cdots + k_i r_d^{2i}) \tag{8}$$

where k_i is the radial distortion coefficients.

A good approximation is to truncate Taylor series in the second coefficient.

C. Salt and Pepper Noise

Impulse or salt and pepper noise is a common image degradation that can badly destroy the information of an image and makes the succeeding image processing a hard or even an impossible task [24]. Its causes come mainly from malfunctioning pixel in image sensors, memory position fault in hardware, timing errors in the process of digitization, or transmission in noisy channels. For our interests, let $f(x,y)$ denotes the pixel gray value of an original image at the position (x,y), and $[L_{min}, L_{max}]$ the dynamic range of gray values of $f(x,y)$, i.e., $[L_{min} \leq f(x,y) \leq L_{max}]$. The model for the corrupted image $g(x,y)$ is described as follows:

$$g(x,y) = \begin{cases} L_{min}, \text{ with probability } p, \\ L_{max}, \text{ with probability } q, \\ f(i,j), \text{ with probability } 1-p-q, \end{cases} \tag{9}$$

where $D = p + q$ defines the noise density.

IV. Experimental Results

Based on (3), we submitted the standard QR code decoder[1] under simulated conditions to analyze its robustness against common distortions aforementioned. The experimental environment is Windows 7 operating system, MATLAB R2014a. We settled our experiments in QR code V2, size 522×522 pixels and error corrector level M. We seek for the minimum peak signal-to-noise ratio (PSNR) in which the QR code is capable to achieve SSR. The SSR is obtained if three conditions are satisfied: 1) finder patterns are located; 2) version and format versions are successfully decoded; and 3) the number of detected errors is lower than the error correction capacity.

PSNR is an objective method to determine the image quality or loss of information. For grey-level (8 bits) images PSNR is defined by [25]:

$$PSNR \triangleq 10 \cdot \log_{10}\left(\frac{255^2}{MSE}\right), \qquad (10)$$

where MSE is the mean square error between a reference image $f(x,y)$ and a test image $g(x,y)$, both of size $(M \times N)$, and expressed by:

$$MSE = \frac{1}{MN}\sum_{x=1}^{M}\sum_{y=1}^{N} \| f(x,y) - g(x,y) \|^2 . \qquad (11)$$

Fig. 6 depicts the minimum tolerable PSNR, i.e. maximum barcode degradation, to each distortion that ensures SSR. Standard QR code is more robust to barrel and pincushion distortions, because they allow a lower PSNR when compared to other distortions. This means that QR code can be strongly corrupted by barrel and pincushion degradation and still achieve SSR. On the other hand, salt and pepper noise reach the worst performance, which seems reasonable once this noise strongly affects the pixels values as seen in (9). We also assess the QR code performance against low contrast[2] images. In this case, we can say that low contrast images emulate low lighting acquisition, or shadowing. As one can see in Fig. 6, QR code has high capacity to minimize contrast reduction.

Furthermore we combined the effect of image contrast reduction with other channel impairments. We started our analysis from 0% of contrast reduction (full contrast) until the last value where we obtained SSR. As shown in Fig. 7, as the contrast reduces SSR can not be assured anymore since (1) fails to correctly locate the function patterns of the QR code. Contrast reduction values, along "x" axis, deteriorate the performance of barrel and pincushion distortions, since PSNR increases to ensure SSR. Otherwise, the remain curves establish an improvement of the performance when QR code has the contrast reduced. Such results show that in some cases combining two kinds of distortions is better than when they are considered isolatedly. For illustration purpose Fig. 6 shows*illustrates* the point where contrast reduction is 0%,

[1]Available in Google open-source 1D/2D barcode image processing library Zxing-2.1.

[2]We analyze only images distorted by uniform contrast, i.e. all image degraded with same contrast value.

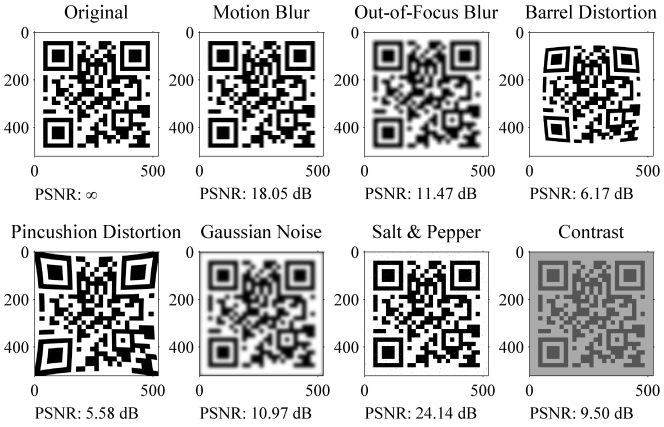

Fig. 6. Simulated standard QR code degradation limits under common distortions. QR code size 522×522 pixels and error corrector level M were considered. White Gaussian blur was settled using a smoothing kernel with size 130×130.

while Fig. 8 shows the exact PSNR and contrast reduction where the minimum SSR is ensured. Therefore, Figs. 6 and 8 are the first and last points in Fig. 7, respectively. In summary, Table I compares the obtained PSNR for the distortions considered in the simulations.

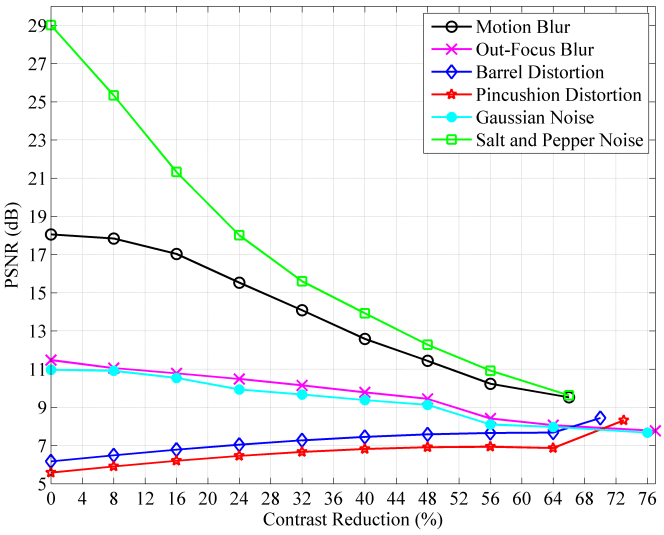

Fig. 7. Combination of contrast reduction and common image degradations. QR code size 522×522 pixels and error corrector level M were considered. White Gaussian blur was settled using a smoothing kernel with size 130×130.

V. Conclusions

This paper presented an overall optical channel model to assess the robustness of standard QR code decoder under typical image degradations which are: motion and defocus blur, lighting reduction, barrel and pincushion distortion, Gaussian and salt and pepper noise. We can say that standard QR code decoder is stronger (in terms of SSR) to barrel and pincushion distortions, but more sensitive to salt and pepper noise. On the other hand, a QR codes impaired by barrel and pincushion distortion have worst performances as long

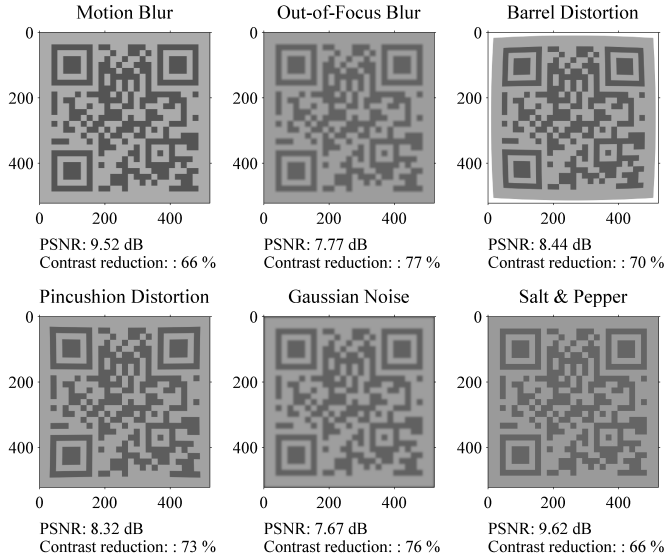

Fig. 8. Minimum contrast values which ensure SSR (simulated). QR code size 522×522 pixels and error corrector level M were considered. White Gaussian blur was settled using a smoothing kernel with size 130×130.

TABLE I

PSNR FOR THE MINIMUM AND MAXIMUM CONTRAST REDUCTION TO EACH CHANNEL IMPAIRMENT.

Distortion	Contrast (%)	PSNR (dB)
Motion blur	0	18.05
	66	9.52
Out-of-focus blur	0	11.47
	77	7.77
Barrel	0	6.17
	70	8.44
Pincushion	0	5.58
	73	8.32
Gaussian noise	0	10.97
	76	7.67
Salt and pepper noise	0	28.95
	66	9.62

as the image contrast reduces. In other words, this means that a combined distortion of barrel and pincushion plus contrast reduction require a higher PSNR to ensure SSR. Future studies should focus on analysis of different QR code versions, errors correction levels and image resolutions.

ACKNOWLEDGMENTS

The authors would like to thank CNPq, CISB, and the Brazilian Army for the financial support.

REFERENCES

[1] T. Falas and H. Kashani, "Two-dimensional bar-code decoding with camera-equipped mobile phones," in *15th Annual IEEE International Conference on Pervasive Computing and Communications Workshops*, pp. 597–600, Mar 2007.

[2] A. Ashok, S. Jain, M. Gruteser, N. Mandayam, W. Yuan, and K. Dana, "Capacity of pervasive camera based communication under perspective distortions," in *International Conference on Pervasive Computing and Communications*, pp. 112–120, Mar 2014.

[3] M. Vizcarra Melgar, M. Farias, F. De Barros Vidal, and A. Zaghetto, "A high density colored 2D-barcode: CQR Code-9," in *29th Conference on Graphics, Patterns and Images*, pp. 329–334, Oct 2016.

[4] ISO/IEC 15420:2009, "Information technology – Automatic identification and data capture techniques – EAN/UPC bar code symbology specification," 2009.

[5] M. M. Rana, M. E. Kawsar, M. E. Rabbani, S. M. M. Rashid, and K. E. U. Ahmed, "An enhanced two-dimensional color barcode system," *Journal of Emerging Trends in Engineering and Applied Sciences*, v. 2, no. 1, pp. 126–131, 2011.

[6] S. Wasule and S. Metkar, "An effective approach to recover corrupted or mobile captured 2D barcode images with improved accuracy," in *Conference on Advances in Signal Processing*, pp. 108–113, Jun 2016.

[7] ISO/IEC 18004:2015, "Information technology – Automatic identification and data capture techniques – QR Code bar code symbology specification," 2015.

[8] S. Tiwari, "An introduction to QR code technology," in *15th International Conference on Information Technology*, v. 1, (Bhubaneswar, India), pp. 39–44, Dec 2016.

[9] L. Belussi and N. Hirata, "Fast QR code detection in arbitrarily acquired images," in *24th Conference on Graphics, Patterns and Images*, pp. 281–288, Aug 2011.

[10] ISO/IEC 16022:2006, "Information technology – Automatic identification and data capture techniques – Data Matrix bar code symbology specification," 2006.

[11] Yunhua Gu and Weixiang Zhang, "QR code recognition based on image processing," in *International Conference on Information Science and Technology*, pp. 733–736, Mar 2011.

[12] M. Kikuchi, M. Fujiyoshi, and H. Kiya, "A new color QR code forward compatible with the standard QR code decoder," in *International Symposium on Intelligent Signal Processing and Communication Systems*, pp. 26–31, Nov 2013.

[13] G. Xu, R. Li, L. Yang, and X. Liu, "Identification and recovery of the blurred QR code image," in *International Conference on Computer Science and Service System*, pp. 2257–2260, Aug 2012.

[14] J.-A. Lin and C.-S. Fuh, "2D barcode image decoding," *Mathematical Problems in Engineering*, v. 2013, p. 10, 2013.

[15] S. Tiwari, V. P. Shukla, S. R. Biradar, and A. K. Singh, "Blur classification using ridgelet transform and feed forward neural network," *International Journal of Image, Graphics and Signal Processing*, v. 6, p. 47, Aug 2014.

[16] H. Bagherinia and R. Manduchi, "A novel approach for color barcode decoding using smart phones," in *IEEE International Conference on Image Processing*, pp. 2556–2559, Oct 2014.

[17] S. Lyons and F. R. Kschischang, "Two-dimensional barcodes for mobile phones," in *25th Biennial Symposium on Communications*, pp. 344–347, 2010.

[18] M. E. Vizcarra Melgar, A. Zaghetto, B. Macchiavello, and A. C. A. Nascimento, "CQR codes: Colored quick-response codes," in *IEEE International Conference on Consumer Electronics*, pp. 321–325, Sep 2012.

[19] R. C. Gonzalez and R. E. Woods, *Processamento Digital de Imagens*. São Paulo: Pearson Prentice Hall, 3ª ed., 2010.

[20] M. E. Moghaddam, "A mathematical model to estimate out of focus blur," in *5th International Symposium on Image and Signal Processing and Analysis*, pp. 278–281, Sep 2007.

[21] S. Tiwari, V. P. Shukla, and A. K. Singh, "Review of motion blur estimation techniques," *Journal of Image and Graphics*, v. 1, no. 4, pp. 176–184, 2013.

[22] G. Vass and T. Perlaki, "Applying and removing lens distortion in post production," in *2nd Hungarian Conference on Computer Graphics and Geometry*, pp. 9–16, 2003.

[23] H. Tian, Y. Xiao, G. Cao, J. Ding, and B. Ou, "Robust watermarking of mobile video resistant against barrel distortion," *China Communications*, v. 13, pp. 131–138, Sep 2016.

[24] G. Xu and Y. Lin, "An efficient restoration algorithm for images corrupted with salt and pepper noise," in *9th International Congress on Image and Signal Processing, BioMedical Engineering and Informatics*, pp. 184–188, Oct 2016.

[25] A. Horé and D. Ziou, "Image quality metrics: PSNR vs. SSIM," in *20th International Conference on Pattern Recognition*, pp. 2366–2369, Aug 2010.